Chow, S. H. *et al.* (2020). *Géotechnique* **70**, No. 8, 720–731 [https://doi.org/10.1680/jgeot.19.TI.017]

Consolidation effects on monotonic and cyclic capacity of plate anchors in sand

SHIAO HUEY CHOW*, ANDREA DIAMBRA†, CONLETH D. O'LOUGHLIN‡, CHRISTOPHE GAUDIN‡ and MARK F. RANDOLPH‡

This study investigated the change in monotonic and cyclic capacity of a plate anchor across different degrees of consolidation in dense sand. To quantify the effect of consolidation on anchor capacity, a framework is introduced and validated using centrifuge model anchor test data. The centrifuge tests considered a rectangular plate loaded at varying rates in dense sand, under both monotonic and irregular cyclic conditions, at a fixed embedment depth and with a horizontal load inclination (at the seabed). In order to vary from drained to undrained conditions, the sand was saturated using both water and a viscous pore fluid with viscosity approximately 700 times higher than water. The anchor's ultimate monotonic capacity in dense sand increased by up to 173% as the consolidation response evolved from drained to undrained with generation of dilation-induced suction. This increase in capacity across the consolidation regime can be adequately quantified using the proposed framework; however, uncertainty arises in achieving the theoretical undrained capacity. Both drained and undrained irregular cyclic loading resulted in anchor capacity increases of up to 33%, attributed to soil volume changes associated with cyclic densification under drained cyclic loading and excess pore pressure dissipation under undrained cyclic loading.

KEYWORDS: anchors & anchorages; centrifuge modelling; offshore engineering; sands

INTRODUCTION

The emergence of offshore floating renewable energy devices requires economic anchoring technology that is effective in sand. Plate anchors are one of the technologies that could satisfy this requirement, although their response to realistic monotonic and cyclic loading under offshore conditions still requires a more robust understanding, particularly under partially drained conditions imposed by varying loading rates. Existing studies have focused on investigating the drained monotonic capacity of plate anchors in sand at a fixed orientation, with loading normal to the plate (e.g. Dickin & Leung, 1983; Murray & Geddes, 1989; Merifield & Sloan, 2006). However, from experience for oil and gas applications, plate anchors are more likely to be installed vertically and allowed to rotate and key (e.g. Chow *et al.*, 2017, 2018a), which results in progressive change of the loading angle at the load attachment point (or 'padeye') and also of the anchor embedment, and consequently the anchor capacity. While the keying process and the associated change in embedment have been well studied for plate anchors in clay (e.g. Gaudin *et al.*, 2009; Song & Hu, 2009; Wang *et al.*, 2011; Cassidy *et al.*, 2012), only limited work has been reported for assessing the keying behaviour of plate anchors in sand (O'Loughlin & Barron, 2012). Moreover, understanding the response of plate anchors in sand to cyclic loading is crucial for design optimisation in offshore renewable energy applications, but has received only limited attention (Bemben *et al.*, 1973; Chow *et al.*, 2015, 2018a). A preliminary assessment of the keying process and the behaviour of plate anchors under both monotonic and irregular cyclic loading in dry dense sand conducted by Chow *et al.* (2015) revealed that vertically embedded anchors underwent similar anchor rotation when the loading was monotonic and cyclic. The study also demonstrated that the drained cyclic ultimate capacity was up to 13% higher than the monotonic ultimate capacity when subjected to a 'storm' of irregular cyclic loading. The increase in capacity can be attributed to the progressive densification of the granular soil surrounding the anchor.

The uncertainty around consolidation effects on plate anchor capacity in sand adds further complexity to the problem. This is demonstrated by a field study of fluke anchors in sand, where the fluke anchor capacity was under-predicted by 40% using finite-element analysis assuming drained conditions, presumably due to consolidation effects (Heurlin *et al.*, 2015). Consolidation effects in sand (encompassing the complete response from drained to undrained) has been relatively well studied experimentally at element level, where drainage can be controlled easily (e.g. triaxial testing by Watanabe & Kusakabe (2013)). However, achieving undrained conditions for boundary value problems such as plate anchors in sand is experimentally challenging due to the high hydraulic conductivity of sand.

This study investigates consolidation effects on the monotonic and cyclic capacity of a vertically embedded rectangular plate anchor in dense sand. A framework is first introduced to define and capture consolidation effects for plate anchors in sand. The framework is then validated using model anchor tests performed in a geotechnical centrifuge. The model rectangular plate anchor, installed vertically and allowed to key by preloading, was loaded at a range of velocities under both monotonic and cyclic loading, at a fixed embedment depth and under horizontal load inclination at the seabed (i.e. mimicking a typical catenary mooring). To reproduce the whole drained to

Manuscript received 28 February 2019; revised manuscript accepted 18 November 2019. Published online ahead of print 20 December 2019.
Discussion on this paper closes on 1 December 2020, for further details see p. ii.
* Centre for Offshore Foundation Systems, University of Western Australia, Perth, WA, Australia (Orcid:0000-0002-5442-0014).
† Department of Civil Engineering, University of Bristol, Bristol, UK (Orcid:0000-0003-4618-8195).
‡ Centre for Offshore Foundation Systems, University of Western Australia, Perth, WA, Australia.

undrained response spectrum during the experimental programme, the sand was saturated using either water or a viscous pore fluid in order to control consolidation conditions.

INTERPRETATION FRAMEWORK

The effect of consolidation conditions or shearing rates ('rate effects') on the plate anchor capacity in sand can be assessed within the well-established 'backbone curve' framework (Fig. 1), whereby the consolidation regime is related to the non-dimensional velocity, $V = vd/c_v$ involving the loading rate (v), the nominal dimension of the anchor (d) and the coefficient of consolidation (c_v) (e.g. Finnie & Randolph, 1994; Bransby & Ireland, 2009; Suzuki & Lehane, 2014; Chow *et al.*, 2018b). For a rectangular geometry, d is often considered (e.g. Chung *et al.*, 2006; Colreavy *et al.*, 2016) as the diameter of an equivalent circle with the same projected area. With increasing non-dimensional velocity, the soil behaviour evolves from drained to partially drained and then undrained. The non-dimensional velocities V_{dr} and V_{un} mark the drained and undrained boundaries, respectively (Fig. 1). In sand, positive or negative effects of partial consolidation with increasing loading rate can be observed depending on the sand dilatancy during shearing, which is governed by the sand density, mineralogy and stress level (Bolton, 1986). For contractive sands, anchor capacity (q) decreases with increasing V in the partially drained region ($V_{dr} < V < V_{un}$) due to positive excess pore pressure generation, while in dilatant sands q increases with increasing V due to negative excess pore pressure generation, also relevant for ploughing, pipelines, dynamically installed anchors and cone penetrometers (e.g. Bransby & Ireland, 2009; Chow *et al.*, 2017; Chow *et al.*, 2018b; Robinson *et al.*, 2019). This change in anchor capacity with V arises from (a) partial consolidation of the surrounding sand during loading, but also from (b) viscous (rheological) effects. Although viscous effects in sand are often assumed to be secondary relative to consolidation, they have been reported to cause between 0 and 10% increase in shear strength per log cycle increase in strain rate (Dayal & Allen, 1975; Watanabe & Kusakabe, 2013). A back-bone curve that captures the change in anchor capacity in sand with increasing loading rate, can be expressed as

$$\frac{q_u}{q_{u(dr,ref)}} = \left[\frac{1 + (q_{u(un)}/q_{u(dr,ref)})(V/V_{50})^c}{1 + (V/V_{50})^c}\right] \times \left[\frac{1 + m\left[(v/d)/(v/d)_{ref}\right]^n}{1 + m}\right] \quad (1)$$

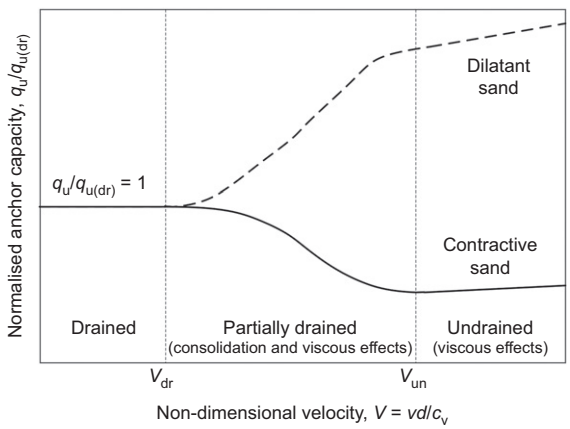

Fig. 1. Framework for interpreting consolidation effects on plate anchor capacity in sand (adapted from Chow *et al.*, 2018b)

adapted from Chow *et al.* (2018b) and Randolph (2016), where q_u is the ultimate anchor capacity corresponding to V or v/d; $q_{u(dr,ref)}$ is the reference ultimate drained capacity at $(v/d)_{ref}$; $q_{u(un)}$ is the ultimate undrained capacity at $V = V_{un}$; V_{50} is the non-dimensional velocity for 50% consolidation; v/d is the loading rate normalised by anchor (equivalent) diameter d; c is a fitting coefficient that governs the curvature of the evolution of $q_u/q_{u(dr,ref)}$; m is a parameter defining the viscous property of the sand; and n is the shear-thinning index which takes into account the viscosity effect and defines the rate of variation of $q_u/q_{u(dr,ref)}$ with respect to the normalised loading rate, v/d.

The first term on the right-hand side of equation (1) accounts for consolidation effects, whereas the second term accounts for viscous effects using the Herschel–Bulkley formulation. The latter is based on non-Newtonian fluid mechanics, and is adopted here to quantify viscous rate effects for its capability (relative to other strain rate formulations) of providing a sensible minimum resistance at zero strain rate (Zhu & Randolph, 2011). Note that the ultimate anchor capacity q_u in equation (1) can also be replaced by its normalised form of anchor capacity factor $N_\gamma = q_u/\gamma' H$ where γ' is the effective unit weight and H is the initial anchor embedment depth from the soil surface to the centroid or padeye of the anchor.

Application of this framework requires the limiting drained and undrained capacities ($q_{u(dr,ref)}$ and $q_{u(un)}$) to be established first, and then the partially drained regime can be defined by fitting equation (1) to experimental data. Depending on the anchor geometry, orientation and loading inclination, the drained anchor capacity ($q_{u(dr,ref)}$) can be estimated using existing solutions (e.g. Murray & Geddes, 1989; Merifield & Sloan, 2006; White *et al.*, 2008), although there may be uncertainties related to the final orientation of an anchor that undergoes keying. Previous experimental studies (Chow *et al.*, 2015) have demonstrated that a rectangular plate anchor with length (L) and width (B), under the test configuration of this study (vertically installed and pulled horizontally at mudline), will experience a rotation of about 54° from the horizontal at ultimate capacity. Hence $q_{u(dr,ref)}$ can be estimated here using existing solutions for inclined strip anchors (e.g. Murray & Geddes, 1989; Bhattacharya & Kumar, 2014), but adjusted by a shape factor (S_f) to account for the rectangular shape of the anchors (Ovesen & Stromann, 1972)

$$q_{u(dr,ref)} = S_f N_\gamma \gamma' H \quad (2)$$

with

$$S_f = 0{\cdot}42\frac{[(H/B) + 1]}{L/B} + 1 \quad (3)$$

The ultimate undrained capacity of the anchor, $q_{u(un)}$, may be expressed through a conventional undrained bearing capacity formulation

$$q_{u(un)} = N_c s_u \quad (4)$$

where N_c is an anchor capacity factor that can be estimated using existing plate anchor solutions in undrained clay (e.g. Merifield *et al.*, 2005). The undrained shear strength of the sand (s_u) may be estimated analytically through critical state concepts (Muir Wood, 1990; Been *et al.*, 1991)

$$s_u = \frac{M}{2} p'_{cs} = \left(\frac{3 \sin \phi_{cs}}{3 - \sin \phi_{cs}} p'_{cs}\right) \quad (5)$$

where $M = 6 \sin\phi'_{cs}/(3 - \sin\phi'_{cs})$ is the deviatoric to isotropic stress ratio in triaxial compression conditions; ϕ'_{cs} is the critical state friction angle, estimated as 31·9° from

triaxial compression tests for the silica sand considered in this study (Chow *et al.*, 2019); and p'_{cs} is the mean effective stress at critical state that can be estimated by equating the Bolton (1986) relative dilatancy index I_R to zero (zero dilation at critical state)

$$I_{R(cs)} = D_r(Q - \ln p'_{cs}) - R = 0 \tag{6}$$

Hence

$$p'_{cs} = e^{Q-R/D_r} \tag{7}$$

In these expressions, D_r is the relative density of the sand; Q and R are two material constants calibrated as 9·6 and 1, respectively, through triaxial compression tests for the silica sand considered in this study (Chow *et al.*, 2019).

If undrained conditions can be achieved in sand, the anchor can generate large undrained capacity in dense sand. However, for offshore renewable energy applications, undrained loading in dense sand in relatively shallow water can lead to cavitation – that is, the formation of vapour bubbles within the pore water (e.g. McManus & Davis, 1997; Palmer, 1999; Byrne & Houlsby, 2002) – which may limit the undrained shear strength and hence the anchor capacity. During cavitation, the sand will dilate with unrestrained volumetric change (just as in the drained response) such that the sand strength is anticipated to revert to an equivalent drained value, but with the negative pore pressure or suction limited by the cavitation pressure (u_{cav}) (McManus & Davis, 1997). Hence the anchor undrained capacity upon cavitation can be quantified as

$$q_{u(un,cav)} = N_\gamma(\gamma H - u_{cav}) \tag{8}$$

where γ is the soil unit weight; $u_{cav} = -f_c p_a = u_w + \Delta u_{cav}$; f_c is a constant indicating the level of cavitation where $f_c \leq 1$ (1 for full cavitation); p_a is atmospheric pressure; u_w is the hydrostatic pressure; and Δu_{cav} is the excess pore water pressure upon cavitation.

A significant limitation of the above is in the estimation of a suitable 'operative' undrained shear strength for the sand, particularly in the presence of cavitation, since the conditions within the failure zone in front of the anchor will involve soil at different stages of shearing, and hence degrees of dilation. In order to explore this, and the relevance of the framework, a series of monotonic anchor pull-out tests were conducted in dense sand covering the complete consolidation regime from drained to undrained, as discussed in subsequent sections.

CENTRIFUGE TEST DESCRIPTION

Scaling considerations

The model tests undertaken are (fast) static tests, rather than dynamic tests. As such, correct scaling of time is governed by consolidation processes, with time scaled as $1/N^2$ where N is the gravitational acceleration scaling factor in the centrifuge (Garnier *et al.*, 2007). Correspondingly, velocity (displacement divided by time) is scaled as N. Assuming that the consolidation coefficient of the soil is identical for model and prototype conditions, the quantity $V = vd/c_v$ is scaled as $N \times (1/N) = 1$. As discussed in the next section, however, for practical considerations it is useful to reduce the coefficient of consolidation for model tests in sand by using viscous pore fluid in order to allow undrained conditions to be achieved with low to moderate velocities.

Modelling concept using viscous pore fluid

In order to allow the consolidation conditions to be varied from drained to undrained, the coefficient of consolidation (c_v), was decreased using a highly viscous pore fluid (as described in Bienen *et al.* (2018), Chow *et al.* (2018b), Robinson *et al.* (2019) and Zhu *et al.* (2019)). The modelling concept of using a viscous pore fluid to satisfy similitude between the physical model and the equivalent prototype is now well accepted in geotechnical physical modelling, specifically in satisfying time scaling for dynamic events (e.g. Stewart *et al.*, 1998; Dewoolkar *et al.*, 1999; Adamidis & Madabhushi, 2015). The coefficient of consolidation (c_v) is directly related to the sand permeability (k) by

$$c_v = \frac{k m_v}{\rho \boldsymbol{g}} \tag{9}$$

where m_v is the compressibility of the soil; ρ is the density of the pore fluid; and $\boldsymbol{g}$ is the Earth's gravitational acceleration. As the sand permeability (k) is inversely proportional to the dynamic viscosity (μ) according to

$$k = \frac{K\rho \boldsymbol{g}}{\mu} \tag{10}$$

where K is the intrinsic permeability of the soil and c_v can be decreased by increasing μ using the viscous pore fluid (Hölscher *et al.*, 2012). As such, the non-dimensional velocity can be increased relative to the value with water as the pore fluid, expressed as

$$V = \frac{vd}{c_v}\frac{\mu}{\mu_{water}} \tag{11}$$

The viscous pore fluid used in this study was methocel cellulose ether Grade F450 with concentration, $C = 2{\cdot}2\%$ ($\mu = 715$ mPas at 20°C measured through viscometer tests, i.e. about 715 times that of water at the same temperature) and its properties can be found in Dow (2002). The methocel F450 was prepared using the 'hot/cold' technique (Dow, 2002; Adamidis & Madabhushi, 2015). Methocel cellulose ether was selected because it produces a similar constitutive behaviour as soil saturated with water, while having a similar density to water (Dewoolkar *et al.*, 1999). Falling head permeability tests confirmed a reduction in permeability by a factor of μ when saturated with methocel (Fangyuan Zhu, personal communication, 2018). Additionally, good agreement was found between two piezocone tests conducted at the same non-dimensional velocity, V, but in samples saturated with different pore fluids: water and methocel F450 (Chow *et al.*, 2018b).

The viscosity of the methocel cellulose ether, a non-Newtonian fluid, depends on the shear rate and temperature. The results of viscometer tests considering a range of concentrations, shear rates and temperatures shows that dynamic viscosity of the methocel decreases with increasing shear rate (Fig. 2). The results agree with those of Dow (2002) despite the small difference in the testing temperature. At low shear rates ($\dot{\gamma} < 40$ s^{-1}), which are higher than those expected in the centrifuge anchor tests ($v/d = 0{\cdot}009$ to $0{\cdot}94$ s^{-1}), insignificant change in viscosity was observed (Fig. 2(a)). A small temperature variation of less than 2°C (19·2 to 21·1°C) was observed in the plate anchor tests and can be accounted for following Adamidis & Madabhushi (2015) (Fig. 2(b)).

Soil properties and preparation technique

Three dense sand samples (S1, S2 and S3) were prepared using a commercially available (Sibelco Australia Limited) fine silica sand with properties as listed in Table 1 and reported further in Chow *et al.* (2019). S1 was saturated with water, and S2 and S3 were saturated with methocel according

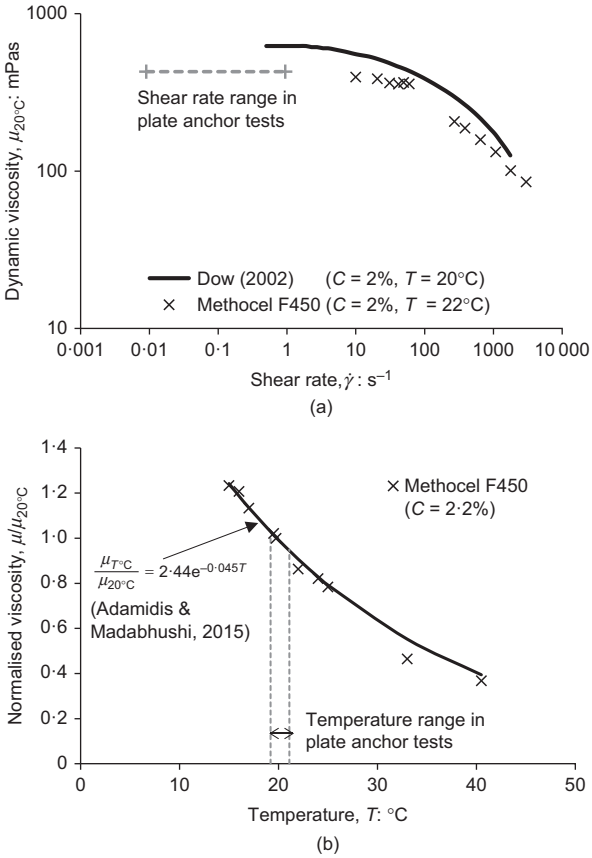

Fig. 2. Variation of methocel viscosity with (a) shear rate; (b) temperature

Table 1. Properties of University of Western Australia (UWA) superfine silica sand (Chow *et al.* 2019)

Specific gravity, Gs	2·67 (Standards Australia, 2006)
Particle size, d_{10}, d_{50}, d_{60}	0·12, 0·18, 0·19 mm (ASTM, 2009)
Minimum dry density, ρ_{min}	1497 kg/m^3 (ASTM, 2006a)
Maximum dry density, ρ_{max}	1774kg/m^3 (ASTM, 2006b)
Coefficient of consolidation, c_v	$c_v = 0{\cdot}00065\ln(\sigma'_v) - 0{\cdot}0015$ (m^2/s) for σ'_v = 20–320 kPa (Rowe cell)
Critical state friction angle, ϕ'_{cs}	31·9° (triaxial)

to the test programme presented in Table 2. The sand samples were prepared using the air pluviation technique into a centrifuge sample container or 'strong box' with internal dimensions of 650 mm × 390 mm × 325 mm (length × width × depth). The sand surface was vacuum levelled to produce a final sample height of approximately 190 mm. The sample was saturated using gravity feed from the base of the sample. More details on the sample preparation and saturation using methocel are discussed in Chow *et al.* (2018b). A ~60 mm layer of water or methocel was maintained above the sand surface during testing. The first two samples (S1 and S2) had a relatively similar relative density, $D_r = 71\%$ and 66% (effective unit weight $\gamma' = 10{\cdot}32$ kN/m^3 and $\gamma' = 10{\cdot}23$ kN/m^3), respectively. The third sample S3 was slightly denser with $D_r = 82\%$ (effective unit weight $\gamma' = 10{\cdot}53$ kN/m^3). This difference in sample density is also reflected in piezocone penetration test results, which were conducted to characterise the samples in the centrifuge at 50$\boldsymbol{g}$.

The piezocone tests were conducted using a 10 mm dia. piezocone instrumented with tip and shaft load cells and a pore pressure transducer at the cone shoulder position (Fig. 3(b)). The piezocone tests were conducted at a penetration velocity, $v = 3$ mm/s, 0·04 mm/s and 0·1 mm/s for samples S1, S2 and S3, respectively. These penetration velocities are expected to produce a drained response (non-dimensional velocity, $V = vd/c_v < 7$) based on the backbone curve established for piezocone tests in the same silica sand (Chow *et al.*, 2018b). The net cone resistance (q_{net}) profiles for the three samples are presented in Fig. 4. The variation in the q_{net} profiles reflects the difference in sample density. Agreeing with the similar sample density measured between S1 and S2, CPT3W ($V = 0{\cdot}06$ in the water-saturated sample) and CPT0·04M ($V = 0{\cdot}75$ in the methocel-saturated sample) produced very similar drained q_{net} profiles. The agreement between the two drained tests further validates the viscosity scaling modelling technique, as observed in Chow *et al.* (2018b). On the other hand, the q_{net} profile in sample S3 (CPT0·1M) is about 30% higher than in samples S1 and S2, confirming that sample S3 was indeed denser.

Model plate anchor and mooring line

A rectangular model plate anchor (see Fig. 3(a)) was used in this study. The anchor was fabricated from stainless steel and sand-blasted such that the interface was close to fully rough (normalised roughness, $R_n = 0{\cdot}09$ as per Dietz (2000)). The plate anchor has an aspect ratio, $L/B = 2$, with length, $L = 40$ mm, width, $B = 20$ mm, plate thickness, $t_a = 4{\cdot}35$ mm and mass, $m_a = 41{\cdot}63$ g. The plate features a triangular-shaped shank with a padeye located at an eccentricity, $e_n = 20$ mm ($e_n/B = 1$) from the plate and along the longitudinal centreline of the line such that the eccentricity perpendicular to the plate is $e_p = 0$ mm. The anchor was instrumented with a 500 kPa capacity pore pressure transducer (Kyowa PS-5KC fitted with a filter). The sensing phase of the transducer was oriented towards the loading direction to measure the pore pressure in front of the anchor. The pore pressure transducer was calibrated (covering positive and negative pressure range) in both methocel and water, with an identical output response observed in both fluids. The anchor was also instrumented with a two-axis micro-electro-mechanical system (MEMS) accelerometer (analogue device ADXL278) with a full-scale range of ±55$\boldsymbol{g}$ in both x- and y-axes to provide a reasonable estimation of anchor rotation (Chow *et al.*, 2015; Chow *et al.*, 2018a; Robinson *et al.*, 2019). Further validation of the anchor rotation derived from the accelerometer measurements was obtained by comparing the accelerometer's measurement with physical measurements made after completion of the anchor tests (as discussed later).

The anchor was pulled using a mooring line that was either a 1 mm or 1·75 mm dia. stainless steel wire, with respective minimum breaking loads of 1·1 kN and 2 kN. The higher rated wire was required in the samples saturated with methocel (S2 and S3) owing to the higher anchor capacities mobilised in these samples.

Experimental arrangement and procedures

The centrifuge tests were carried out at 50$\boldsymbol{g}$ using the 3·6 m dia. beam centrifuge at UWA. The centrifuge test programme is summarised in Table 2, and comprised nine monotonic and three irregular cyclic tests in the three dense sand samples saturated with water (S1) and methocel (S2 and S3). No more than six anchor tests were conducted in each centrifuge sample with sufficient distance allowed between each test site. Lack of interference between tests is demonstrated by the repeatability observed between identical tests conducted within the same sample (more details in the 'Results' section). All anchor tests involved an initially vertical

Table 2. Centrifuge anchor test programme and results

Test series*		T: °C	μ: mPas	v: mm/s	V	q_u: kPa	N_γ	δ_u/B	α_u: deg	u_u: kPa	$\Delta z_f/B$
Dry§ ($\gamma' = 16{\cdot}43$ kN/m^3) (Chow *et al.* 2015)	M0·1D	—	0	1	0	728·4	8·9	2·96	66·8	—	—
	IC1D	—	0	3	0	825·2	10	2·65	63·8	—	—
	IC1·25D	—	0	3	0	820·3	10	2·94	66·3	—	—
	IC1·5D	—	0	3	0	712·0	8·7	2·75	62·1	—	—
S1 (water), $\gamma' = 10{\cdot}32$ kN/m^3, $c_v = 4{\cdot}93 \times 10^{-4}$ m^2/s at $z = 2{\cdot}8$ m	M0·3W(1)†	—	1	0·3	0·02	445·7	8·6	4·41	—	—	—
	M0·3W(2)	—	1	0·3	0·02	439·8	8·5	4·11	55·3	65·1	2·67
	IC1W	—	1	30	1·95	583·7	11·3	3·70	47·3	75·3	1·65
	IC1·25W‡	—	1	30	1·95	509·9	9·9	3·88	52·8	64·9	1·56
S2 (methocel), $\gamma' = 10{\cdot}23$ kN/m^3, $c_v = 7{\cdot}3 \times 10^{-7}$ m^2/s** at $z = 2{\cdot}8$ m	M30M	19·2	743	30	1349	1201·7	23·5	5·02	54·7	12·8	2·90
	IC1M	20·3	707	30	1276	1529·2	29·9	4·94	53·4	0·5	2·66
S3 (methocel) $\gamma' = 10{\cdot}53$ kN/m^3, $c_v = 5{\cdot}99 \times 10^{-7}$ m^2/s at $z = 2{\cdot}8$ m	M0·3M	21·1	675	0·3	16	687·1	13·1	4·03	52·3	51·6	2·47
	M1M	20·4	703	1	55	802·9	15·3	4·34	52·3	41·6	2·88
	M3M	21·1	678	3	158	1067·0	20·3	5·11	53·7	18·1	2·60
	M10M(1)‡	20·9	684	10	533	1552·7	29·5	6·27	60·1	−12·3	2·74
	M10M(2)‡	20·6	693	10	540	1522·8	28·9	6·05	59·7	−19·1	2·56
	M30M‡	20·9	682	30	1595	1497·6	28·5	5·99	59·7	−9·7	2·48

*For ease of reference, tests are identified as $LvP(n)$, where
(*a*) 'L' denotes the loading type (M for monotonic loading, IC for irregular cyclic loading)
(*b*) 'v' denotes the monotonic loading rate ($v = 0{\cdot}3$ to 30 mm/s) or the peak cyclic load ratio ($\mathrm{CLR}_{peak} = q/q_u = 1$ or 1·25)
(*c*) 'P' denotes the pore fluid (D for dry, W for water, M for methocel)
(*d*) 'n' denotes the test recurrence ('1' for the first test, '2' for the second test etc.).

†PPT and/or accelerometer data lost due to damaged cable.
‡Test stopped due to actuator hitting displacement limit.
§Drained monotonic and cyclic test results for a plate anchor with similar geometry (except $t_a = 2{\cdot}75$ mm) in dry dense sand.
**$c_v = c_v\, \mu_{water}/\mu$.

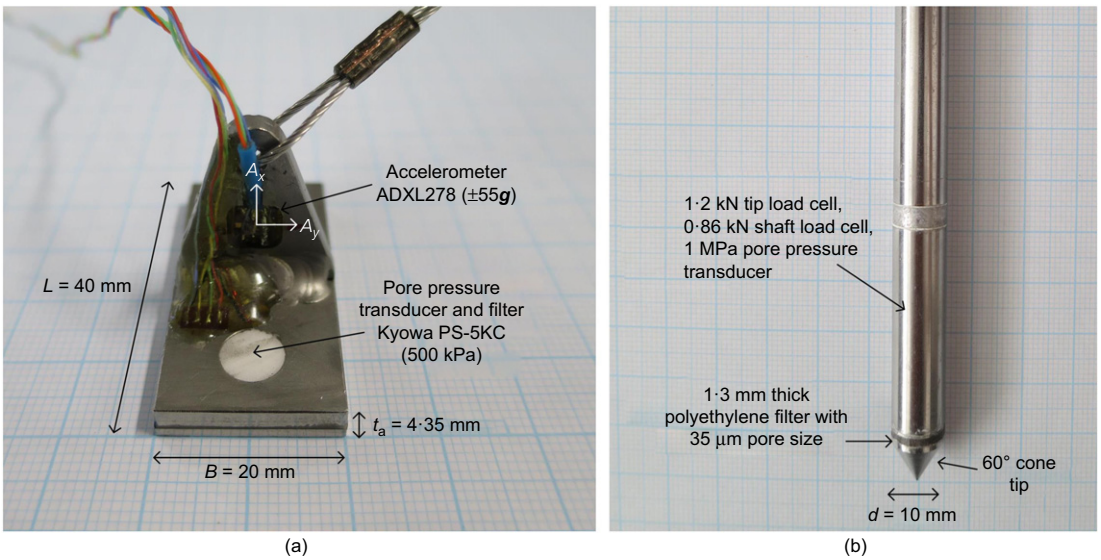

Fig. 3. (a) Model plate anchor; (b) model piezocone

anchor at a normalised embedment depth, $H/B = 5$ (selected to achieve the targeted shallow behaviour and to allow for comparisons with other datasets, e.g. O'Loughlin & Barron (2012)), loaded horizontally at the mudline (i.e. replicating a catenary mooring). The test set-up utilised two electrical actuators, as shown in Fig. 5. After saturating the pore pressure transducer on the anchor, the anchor was penetrated vertically to the targeted depth of 100 mm at 1***g***, using an installation tool attached to the vertical axis of the first actuator. The installation was carried out at 1***g*** as the installation resistance at the testing acceleration of 50***g*** would have been beyond the capacity of the actuator. The installation at 1***g*** may affect the initial stiffness of the anchor load–displacement curve, but is expected to have minimal effect on the anchor ultimate capacity, which occurred at a normalised line displacement, $\delta_u/B \geq 3{\cdot}7$ (Table 2), taking the anchor well away from its initial position and installation site (Fig. 6). The mooring line was then connected to the second actuator by way of a pulley located at the mudline directly beneath the vertical axis of the second actuator, such that the mooring line was maintained horizontal and along the mudline during loading. The centrifuge was then spun to 50***g*** for extraction of the installation tool, followed by monotonic or cyclic loading of the anchor. The rationale for removing the installation tool at 50***g*** was to counter the tendency for the plate anchor to displace upwards with the installation tool if the tool was to be extracted at 1***g*** (Chow *et al.*, 2018a).

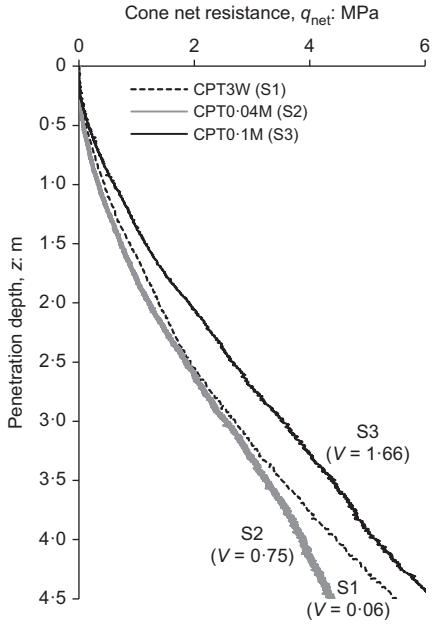

Fig. 4. Piezocone drained net cone resistance profiles across samples S1 to S3

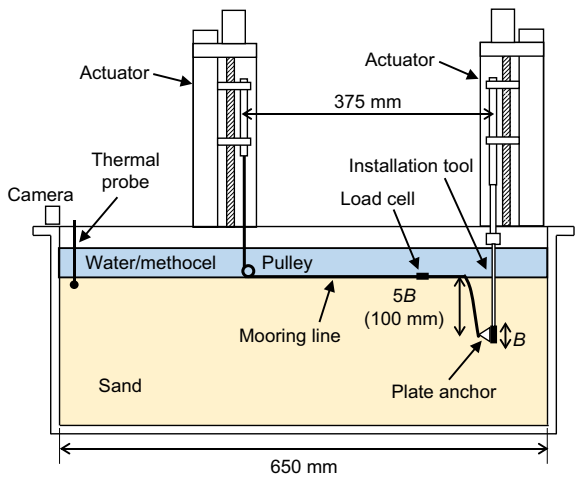

Fig. 5. Centrifuge test set-up

For the monotonic loading tests, the anchor was loaded under displacement control with mooring line velocities, v between 0·3 and 30 mm/s. The cyclic loading tests were conducted under load control using an irregular cyclic loading sequence with different peak cyclic load ratios, $CLR_{peak} = q_{peak}/q_u$, where q_{peak} is the imposed peak cyclic load and q_u is the anchor capacity measured in the corresponding monotonic test under the same consolidation conditions (i.e. drained or undrained loading). If the anchor did not fail at the end of the cyclic sequence, the anchor was loaded monotonically to failure under displacement control.

At the end of each anchor test the anchor was left in the soil until the excess pore pressure was fully dissipated. The centrifuge was then spun down and the anchor was extracted from the sample to be reused for the next test. For the last anchor test in sample S1 the anchor was left in the soil and the longitudinal side wall of the strongbox was removed. The sand was then excavated to expose the anchor position and validate the anchor rotation and loss in embedment established from the accelerometer and pore pressure transducer measurements (see Fig. 6).

ANCHOR TEST RESULTS

Key results from the anchor tests are summarised in Table 2. The quantities, which relate to the point of ultimate anchor capacity, are: anchor capacity (monotonic, cyclic or post-cyclic) (q_u), anchor capacity factor (N_γ), the corresponding normalised mooring line displacement (δ_u/B), anchor rotation (α_u) and pore water pressure (u_u). The dimensionless anchor capacity factor ($N_\gamma = q_u/\gamma' H$) is expected to be slightly conservative, as the depth to the centroid (H) will become progressively more shallow during loading. The loss in anchor embedment (Δz) can be estimated in the drained tests from the change in pore pressure measurement relative to the anchor initial position. For partially drained and undrained tests, only the loss in anchor embedment at the end of the test $\Delta z_f = (u_f - u_i)/\gamma_w$ (the subscripts i and f indicate the initial and final anchor position, respectively, and γ_w is the unit weight of the pore fluid at the testing acceleration) can be estimated after full dissipation of excess pore water pressure.

The accuracy of the accelerometer-based rotation measurement technique was verified by comparing the rotation, α_u (measured relative to the horizontal) established from the accelerometer with the post-test visual examination of the anchor position. As shown in Fig. 6 (test IC1·25W, S1),

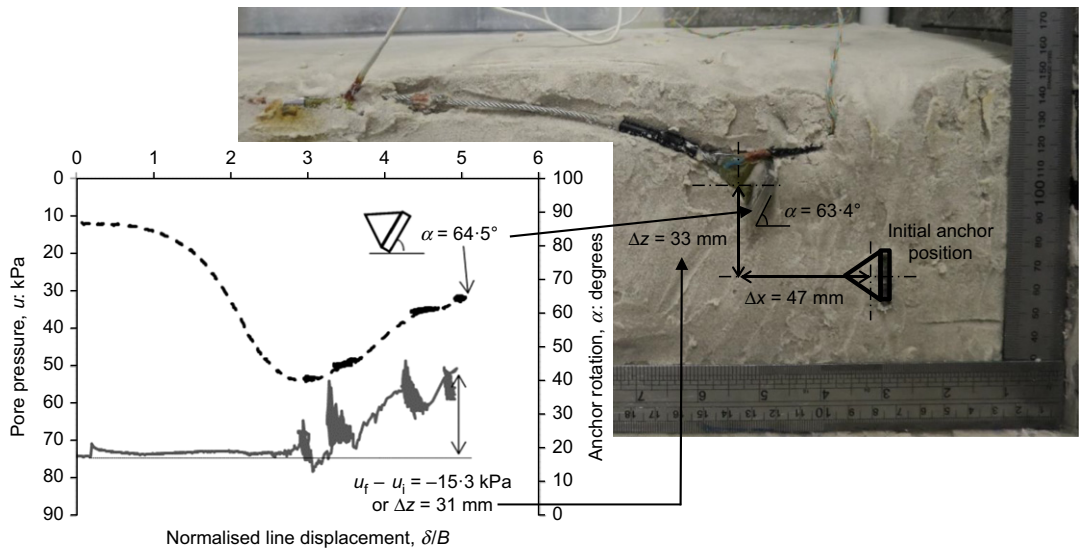

Fig. 6. Validation of anchor rotation and loss in embedment measurements through post-test visual examination of anchor (test IC1·25W)

the difference in rotation between the two approaches is only 1·1°, with the accelerometer yielding a slightly higher angle ($\alpha_u = 64{\cdot}5°$) than the physical measurement ($\alpha_u = 63{\cdot}4°$). The post-test visual assessment of the loss in anchor embedment ($\Delta z = 33$ mm) is also in close agreement with that established from pore water pressure measurements, which gave $\Delta z = (u_f - u_i)/\gamma_w = 31$ mm.

Monotonic capacity investigation

The monotonic test programme served two purposes: (a) to validate the interpretation framework; and (b) to quantify a reference load for the cyclic tests. Selected tests were repeated, and consistent and repeatable test results were obtained (see tests M0·3W and M10M in Table 2). Fig. 7 provides a complete test result from a typical drained monotonic anchor test (test M0·3W(2)). The load–displacement response is typical of that reported previously (e.g. Chow *et al.*, 2015), and can be considered to have four distinctive stages. In stage 1, the load–displacement response is relatively soft as the mooring line starts to cut through the soil. As the anchor starts to rotate (from $\alpha = 86{\cdot}5$ to 70°), load starts to develop with no loss in anchor embedment (Fig. 7(b)). During stage 2 a stiffer load–displacement response is observed as more of the load transferred through the mooring line causes rotation of the plate rather than further cutting of the mooring line through the soil. At the end of stage 2, the anchor has completed keying achieving a peak plate rotation of 42° with a corresponding anchor capacity of about 70% of the ultimate monotonic capacity. In stage 3, the anchor starts to move upward and rotates back towards its initial vertical orientation, since it is easier for the mooring line to further cut through the sand than for the anchor to continue to rotate (Chow *et al.*, 2015). At this stage the mooring line becomes near-normal to the plate and the anchor capacity peaks at a rotation, $\alpha_u = 55°$. Finally, during stage 4 anchor rotation continues to decrease as the load reduces, eventually reaching $\alpha = 75°$ with a corresponding normalised loss in anchor embedment, $\Delta z/B = 2{\cdot}6$, at which point the test was stopped.

The monotonic tests conducted at various loading rates are grouped according to samples (density) as presented in Figs 8 and 9. Fig. 8 shows the three monotonic tests conducted in samples S1 (water saturated) and S2 (methocel saturated) considering two non-dimensional velocities, $V = vd/c_v = 0{\cdot}02$ and 1349. The non-dimensional velocity (V) is computed for each test by considering the coefficient of consolidation (c_v) at the relevant stress level and relative density (indicated for each sample in Table 2). The three tests exhibit similar load–displacement responses, although a stiffer initial response is observed for the tests with the larger diameter mooring line (diameter of 1·75 mm rather

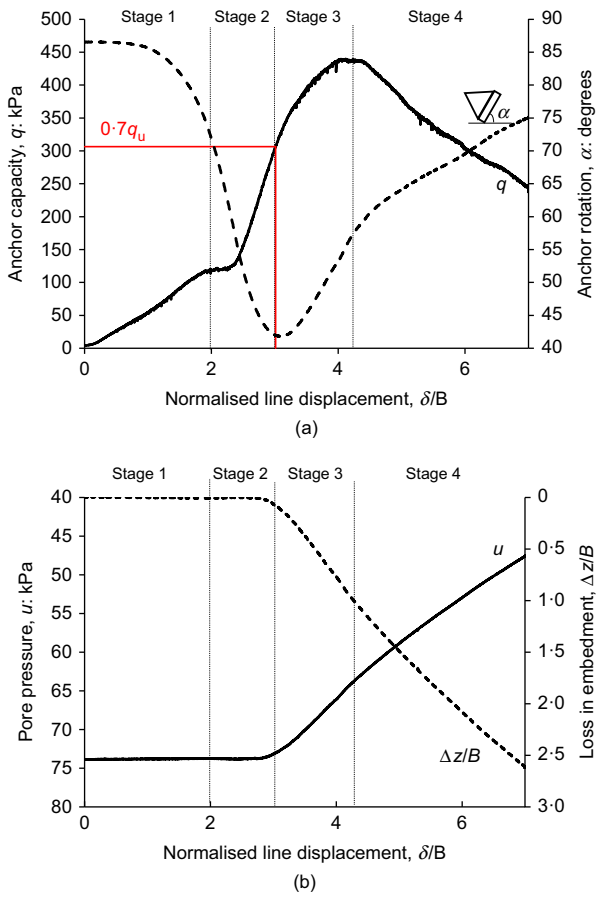

Fig. 7. Typical drained anchor test results (test M0·3W(2))

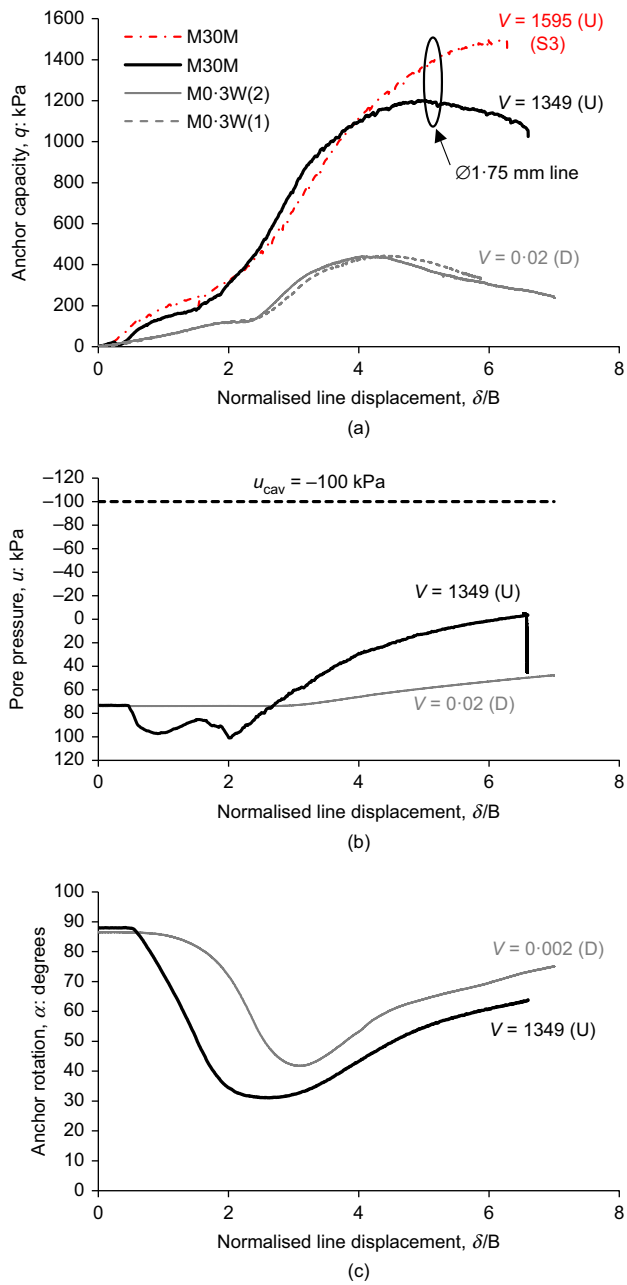

Fig. 8. Monotonic anchor test results for sample S1–S2: (a) load–displacement; (b) pore pressure profiles; (c) anchor rotation at various non-dimensional velocities

than 1 mm). This is to be expected as the higher contact area between the line and the sand would develop higher frictional and bearing resistance, as confirmed through the similar initial stiffness observed in the other set of tests using the 1·75 mm dia. wire in sample S3 (Fig. 9(a)).

The pore pressure profiles in Fig. 8(b) show that tests at $V = 0{\cdot}02$ were drained, while the test at $V = 1349$ exhibits a partially drained to undrained response. For the undrained test ($V = 1349$), excess pore water pressure was positive during anchor keying ($\delta/B < 2{\cdot}7$) before becoming negative as the anchor continued to move upwards. The dilation-induced negative excess pore water pressure resulted in a significant increase in the ultimate anchor capacity (q_u), from 440 to 1202 kPa (i.e. by 173%, see Table 2) as V increases from 0·02 to 1349. At the end of the undrained test, the pore water pressure had fully dissipated back to the hydrostatic value.

More monotonic tests covering a wider range of non-dimensional velocities ($V = 16$ to 1595) were conducted in sample S3 to further explore the consolidation regime (Fig. 9). The pore pressure profiles in Fig. 9(b) show that the slowest test in the methocel-saturated sample (M0·3M) at $V = 16$ gave a similar drained response as test M0·3W ($V = 0{\cdot}02$) in the water-saturated sample (Fig. 7). For the two fastest tests ($V = 540$ and 1595), the capacity started to plateau (Fig. 9(a)) as the test was stopped upon reaching the displacement limit of the actuator ($\delta/B \sim 6{\cdot}5$). Hence the anchor ultimate capacity (q_u) is taken at the final point of the test, $\delta/B \sim 6{\cdot}5$ for these two tests. This is considered to be a reasonable assumption as the load–displacement response at this point is very similar to the other tests where ultimate anchor capacity was clearly observed. As V increases from 16 to 1595, the anchor ultimate capacity (q_u) increases by 118% from 687 to 1498 kPa (Table 2) due to the dilation-induced negative excess pore pressure. The similar q_u observed for the two tests with $V \geq 540$ ($v = 10$ mm/s) suggests that the undrained limit may have been reached, which confirms the undrained response observed earlier for test M30M with $V = 1349$ in sample S2.

The anchor rotation profiles occupy a tight band with 4·8° difference in the peak rotation angle (at the end of keying) across the tests with various loading rates (Fig. 9(c)). Although to a lesser degree than what was observed in S1, there is an apparent decrease in the peak rotation angle as V transitions from drained to undrained. Despite the slight difference in anchor rotation, the anchor underwent a similar loss in embedment with an average $\Delta z_f/B = 2{\cdot}62$ (Table 2).

The variation in normalised anchor capacity, $q_u/q_{u(dr,ref)}$ with non-dimensional velocity in sample S3 is examined using the proposed framework (equation (1)) as shown in Fig. 10. Equation (1) is able to provide a reasonable fit to the experimental data with parameters, $q_{u(un)}/q_{u(dr,ref)}$, V_{50}, c, m and n best fitted as 2·2, 175, 1·3, 0·35 and 0·05, respectively. The respective contributions of the consolidation and viscous components are also presented in Fig. 10. The viscous component ($m = 0{\cdot}35$, $n = 0{\cdot}05$) considers a 4% increase in capacity per log cycle increase in V, as informed from recent laboratory penetrometer testing (unpublished) in this sand. Hence for most problems viscous effects will be minor relative to those due to consolidation, such that the viscous component of equation (1) may be ignored.

The consolidation boundaries, V_{dr} and V_{un} are established as 16 and 540, respectively, based on the range of V investigated in these experiments. The reference drained capacity, $q_{u(dr,ref)} = 687$ kPa ($N_\gamma = 13{\cdot}1$) is taken at $V_{dr(ref)} = 16$ ($v_{ref} = 0{\cdot}2$ m/s, equivalent anchor diameter $d = 0{\cdot}032$ m and a depth averaged $c_v = 4{\cdot}11 \times 10^{-4}$ m^2/s). The measured $N_\gamma = 13{\cdot}1$ is 37% lower than $N_\gamma = 17{\cdot}9$, obtained by scaling the solution for a fully rough strip anchor (at $H/B = 5$, $\alpha = 52°$

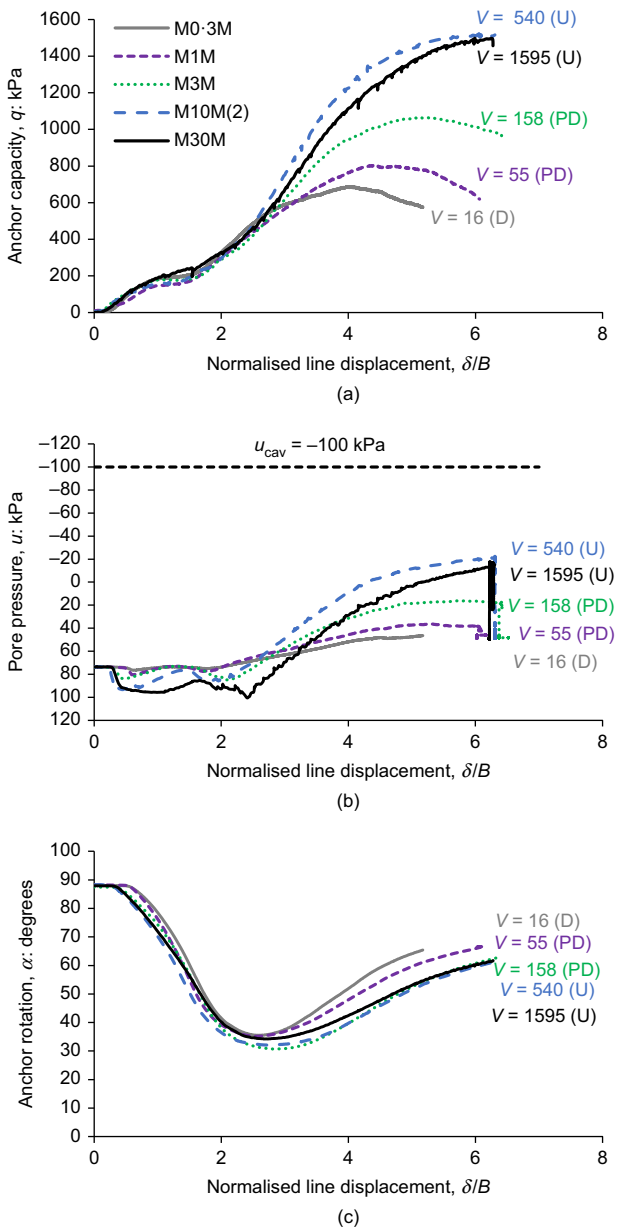

Fig. 9. Monotonic anchor test results for sample S3: (a) load–displacement; (b) pore pressure; (c) anchor rotation profiles at various non-dimensional velocities

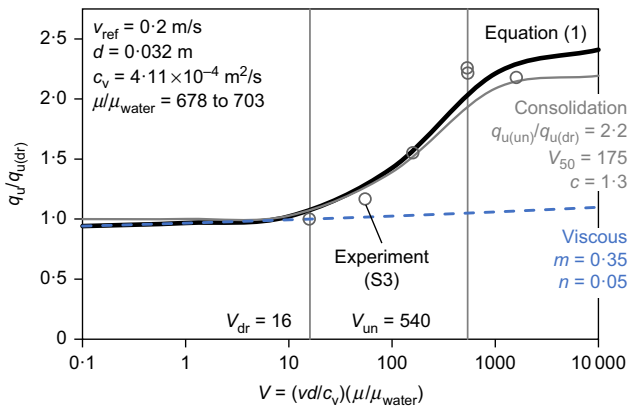

Fig. 10. Validation of framework and best-fit parameters

and $\phi = 40°$), $N_{\gamma(\text{strip})} = 7{\cdot}93$ (Bhattacharya & Kumar, 2014) by a shape factor, $S_f = 2{\cdot}26$ (Ovesen & Stromann, 1972). The higher prediction could be related to: (*a*) the associative flow assumption in the limit analysis by Bhattacharya & Kumar (2014); (*b*) the uncertainty in the shape factor; and/or (*c*) the lack of consideration of the installation effects on the anchor keying stage in the experiment.

The undrained capacity, $q_{u(un)} = 1523$ kPa (test M10M(2)) is taken at $V_{un} = 540$, which is an order of magnitude lower than the predicted $q_{u(un)} = 17\,600$ kPa based on the theoretically estimated $s_u = 2880$ kPa and $N_c = 6{\cdot}11$ for a shallow anchor inclined at $\alpha = 60°$ (Merifield *et al.*, 2005) following equations (4) and (5). It is also worth noting that the measured $q_{u(un)} = 1523$ kPa is 3 times lower than $q_{u(un,cav)} = 4483$ kPa predicted using equation (8). This is consistent with pore pressure measurements confirming that cavitation did not occur (at least adjacent to the anchor, as the localised pore pressure measurement may not truly reflect the complete pore pressure field within the failure zone of the anchor). As shown in Figs 8(b) and 9(b), the most negative excess pore pressure is $u = -19$ kPa, which is higher than the expected cavitation pressure, $u_{cav} = -f_c p_a = -100$ kPa (assuming $f_c = 1$). The much lower measured $q_{u(un)}$ in dense sand reflects differences between element response and boundary value problems, noting that in dense sand very large strains are needed to mobilise ultimate strength (e.g. Verdugo & Ishihara, 1996; Chu *et al.*, 2015; Pan *et al.*, 2018), which may not be attained in the plate anchor failure mechanism. Furthermore, the assumption that all soil elements involved in the failure mechanism exhibit the same simultaneous dilatant response is too simplistic as an hypothesis.

Cyclic capacity investigation

The cyclic test programme and key results from this programme are summarised in Table 2. Two irregular cyclic tests considering peak cyclic load ratios, $CLR_{peak} = 1$ and 1·25, were conducted in the water-saturated sample (S1) to demonstrate the effect of peak cyclic load amplitude on the cyclic anchor capacity. Another cyclic test with $CLR_{peak} = 1$ was conducted in the methocel-saturated sample (S2) to investigate the effect of consolidation on the cyclic anchor capacity. A typical irregular cyclic loading sequence (test with $CLR_{peak} = 1$) is illustrated in Fig. 11. The anchor was first preloaded under displacement control at $v = 30$ mm/s to 70% of its monotonic capacity (CLR = 0·7), followed by a 5 min pause while switching over to the irregular cyclic load sequence under load control with a maximum velocity of 100 mm/s. The CLR = 0·7 preload was selected on the basis that the maximum anchor rotation occurred at this load level, as indicated by the peak anchor rotation measurements (Fig. 7(a)). If the anchor did not fail during cyclic loading, the anchor was loaded monotonically (again after a 5 min pause) under displacement control at $v = 30$ mm/s to measure the post-cyclic ultimate anchor capacity. The minimum cyclic load was taken as 0·020 kN ($q = 25$ kPa) to avoid issues with the load control algorithm trying to achieve zero load.

The irregular cyclic load sequence (Fig. 11) was scaled from mooring line load measurements made in wave tank tests on a wave energy converter with catenary moorings (Casaubieilh *et al.*, 2015) and used in previous plate anchor studies in sand (Chow *et al.*, 2015, 2018a). The original wave load–time series had a total duration of 4083 s (~68 min) and measures a mean wave period, $t_z = 14{\cdot}85$ s, through zero crossing analysis. In the centrifuge tests, a period of $t_z = 1{\cdot}48$ s was adopted in the load-controlled testing, which is the fastest possible rate while maintaining satisfactory load control. Although the response was drained in the water-saturated sample, this test period ($t_z = 1{\cdot}48$ s) led to undrained conditions within each cycle in the methocel

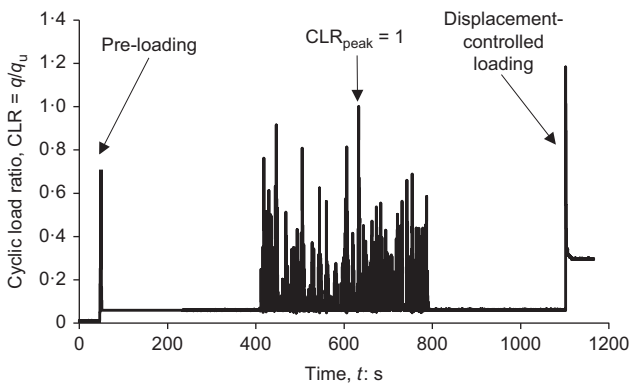

Fig. 11. Applied irregular cyclic load sequence

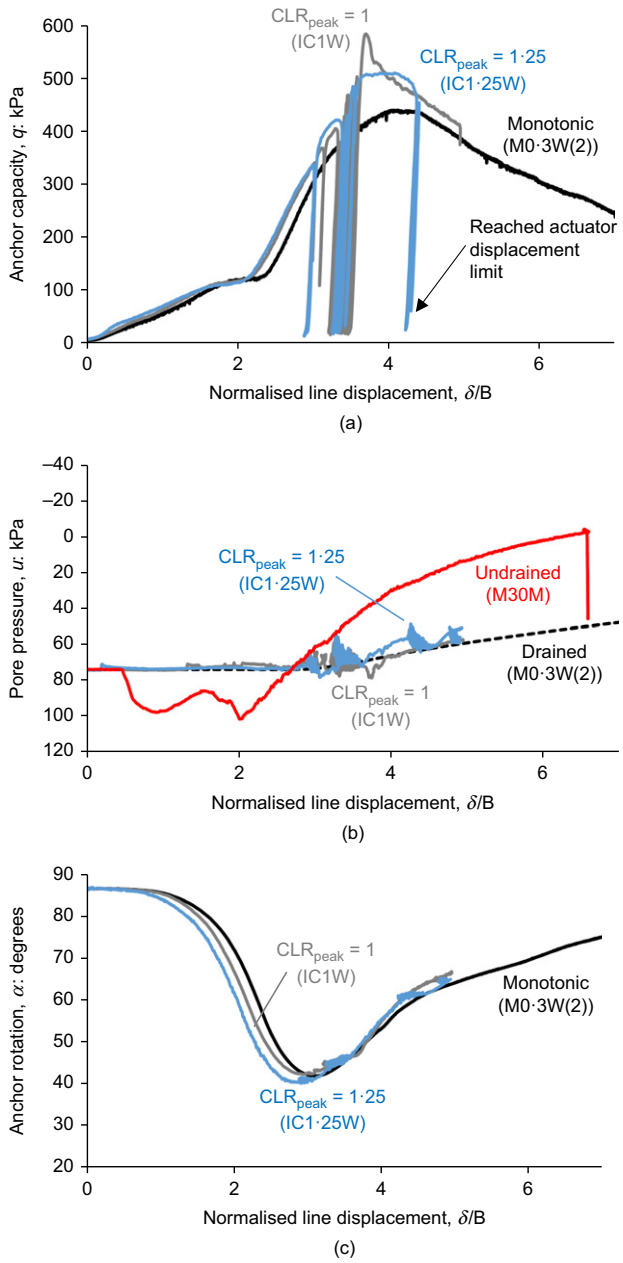

Fig. 12. Effect of CLR_{peak} on anchor capacity: (a) load–displacement; (b) pore pressure; (c) anchor rotation profiles

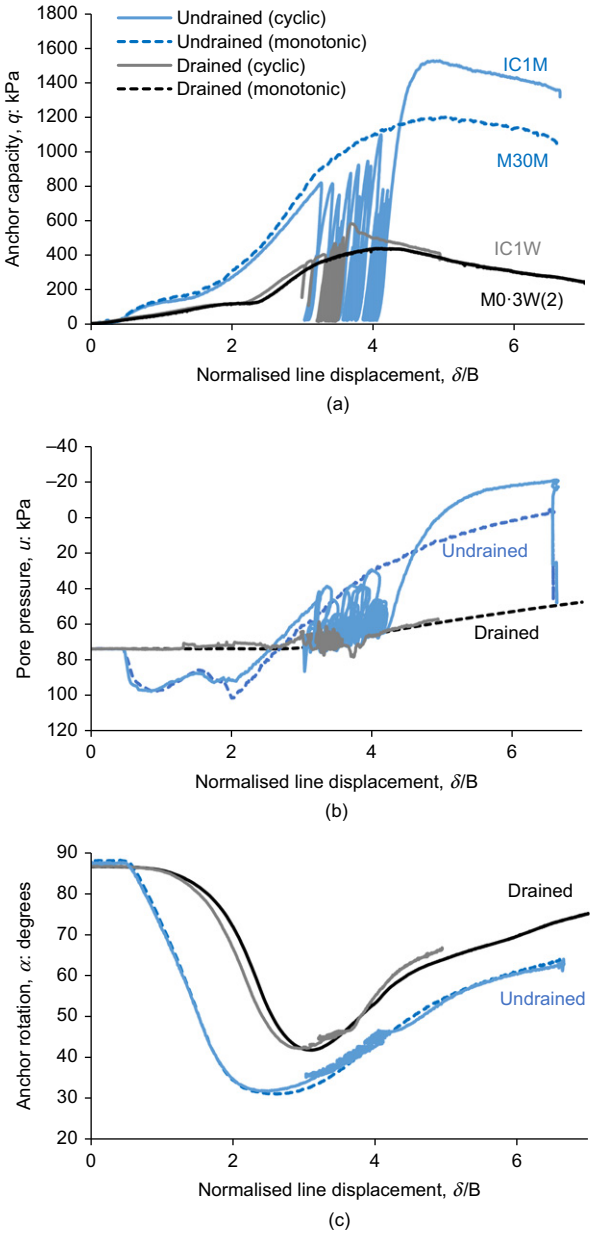

Fig. 13. Effect of consolidation on cyclic capacity of anchor: (a) load–displacement; (b) pore pressure; (c) anchor rotation profiles

saturated sample, as evident in the measured pore pressure responses in Figs 12 and 13, respectively.

The effect of CLR_{peak} on cyclic anchor capacity is presented in Fig. 12, together with the reference monotonic tests. The cyclic tests with the lowest CLR_{peak} (= 1) did not fail during cyclic loading and gave a post-cyclic ultimate anchor capacity ($N_\gamma = 11{\cdot}3$) that is 33% higher than the reference monotonic ultimate capacity ($N_\gamma = 8{\cdot}5$). The test with $CLR_{peak} = 1{\cdot}25$ did not fail during cyclic loading, although the anchor displacement was significant. As a result, the actuator reached its displacement limit at the end of the cyclic loading. However, the maximum load was higher than for the monotonic response, indicating that the cyclic loading had resulted in an increase in soil strength.

It is also noteworthy that the load–displacement curves and the anchor rotation profiles in both cyclic tests are bound by the reference drained monotonic test. These observations are similar to those made from drained cyclic anchor tests reported in Chow *et al.* (2015), which involved an identical test configuration but were in dry sand (results also included in Table 2 for comparison). With increasing CLR_{peak}, increasing negative excess pore pressure is observed for the cyclic tests (see Fig. 12(b)) (undrained test (M30M) also included for comparison). Higher gains in anchor capacity (21 to 33%) are observed here compared to the Chow *et al.* (2015) study in dry sand, which reported capacity gains of up to 13%.

The effect of consolidation on cyclic capacity is demonstrated through the tests involving $CLR_{peak} = 1$ in the water- (drained) and methocel- (undrained) saturated samples as presented in Fig. 13. Neither test failed during cyclic loading and the undrained cyclic test (IC1M) gave a post-cyclic ultimate anchor capacity that is 2·6 times the drained cyclic test (IC1W). When compared to their reference monotonic tests, the drained and undrained cyclic tests gave similar gains in capacity of 33% and 27%, respectively. The higher cyclic capacity is provided by the soil densification under drained cyclic loading (Chow *et al.*, 2015) or associated with excess pore water pressure dissipation after partially drained or undrained cyclic loading. The pore water pressure profiles show that the supposedly drained test (IC1W) generated slight excess pore water pressure during cyclic loading, although this dissipated before the post-cyclic monotonic loading stage of the test as the response during this latter stage was drained (see Fig. 13(b)). In contrast, the undrained test (IC1M) generated significant excess pore water pressure during cyclic loading, with the pore water pressure response bound between those in the drained and undrained monotonic tests. However, during the post-cyclic monotonic loading to failure, the negative excess pore water pressure exceeded the monotonic pore pressure profile. This explains the high post-cyclic ultimate capacity, which was sustained well above the reference undrained monotonic response (M30M).

As shown in Fig. 13(c), the undrained cyclic test also produced a similar anchor rotation profile to that in the reference undrained monotonic test. Greater anchor rotation is observed when the consolidation condition changes from drained to undrained (Fig. 13(c)). Despite the difference in anchor rotation, the loss in embedment is similar in the drained and undrained tests, indicated by the full dissipation of the excess pore pressure at the end of the undrained tests, with the response merging with that in the drained test (Fig. 13(b)).

CONCLUSIONS

A framework is introduced to capture the effect of consolidation on plate anchor capacity in sand. The framework employs the established backbone curve concept and has been further extended to consider the possible occurrence of cavitation, a feature that is considered relevant for offshore renewable energy applications. The framework is validated through a series of centrifuge model anchor experiments in dense sand (representing the most likely seabed state in shallow water), where the different consolidation regimes are reproduced by varying the loading rate and the viscosity of the pore fluid to reduce the sand permeability. The centrifuge tests reveal that, in dense sands ($D_r \sim 82\%$), the anchor monotonic capacity can increase by up to 173% when transiting from drained to undrained conditions, which occurs within an order of magnitude change in the non-dimensional velocity, $V = vd/c_v$ ($V_{dr} = 16$ and $V_{un} = 540$). The measured undrained anchor capacity is found to be only about 33% of that predicted assuming excess pore pressures corresponding to the cavitation limit. Indeed, cavitation was not observed (at least adjacent to the anchor) since the maximum negative excess pore pressure was only about 10% of the theoretical cavitation. Hence, these results highlight

the need for an improved methodology to predict undrained anchor capacity in dense sand. Consistent with previous studies, cyclic loading is found to increase the anchor capacity in dense sand up to 33% when compared to the reference monotonic test. This is a consequence of the soil densification during drained cyclic loading and associated with excess pore pressure dissipation during or after partially drained or undrained cyclic loading. Similar to the monotonic tests, the anchor cyclic capacity increases by 162% when the consolidation condition changes from drained to undrained. The anchor rotation measurement in this study also sheds light on the anchor keying behaviour. The monotonic and cyclic anchor responses are found to produce identical anchor rotation and loss in anchor embedment under the same consolidation conditions.

ACKNOWLEDGEMENTS

This work forms part of the activities of the Centre for Offshore Foundation Systems (COFS), currently supported as a Centre of Excellence by the Lloyd's Register Foundation. The Lloyd's Register Foundation invests in science, engineering and technology for public benefit, worldwide. The work is also supported by the Australian Research Council Discovery Grant Scheme DP190100914, and a Research Collaboration Award provided by the University of Western Australia.

NOTATION

A	anchor bearing area
A_x	acceleration measured in the x-axis
A_y	acceleration measured in the y-axis
B	width of plate anchor
C	concentration of methocel
$\mathrm{CLR}_{\mathrm{peak}}$	peak cyclic load ratio (cyclic peak load over monotonic peak load ratio)
c	a fitting coefficient in equation (1)
c_{v}	coefficient of consolidation
D_{r}	relative density
d	anchor diameter
d_{10}, d_{50}, d_{60}	sand particle size at 10%, 50% and 60% passing, respectively
e_{n}	padeye eccentricity normal to the anchor
e_{p}	padeye eccentricity parallel to the anchor
f_{c}	a constant indicating the level of cavitation
G_{s}	specific gravity
$\boldsymbol{g}$	gravitational acceleration
H	initial anchor embedment depth from soil surface to the centroid or padeye of the anchor
H/B	anchor embedment ratio
I_{R}	Bolton's relative dilatancy index
K	intrinsic permeability of the soil
k	sand permeability
L	plate anchor length
L/B	plate anchor aspect ratio
m, n	viscous property, shear-thinning index in equation (1)
m_{a}	anchor mass
N	gravitational acceleration scaling factor in the centrifuge
N_{c}, N_{γ}	anchor capacity factors
P_{a}	atmospheric pressure
p'_{cs}	mean effective stress at critical state
Q, R	Bolton's material constants
q	anchor capacity
q_{c}, q_{net}	cone resistance, cone net tip penetration resistance
q_{peak}	imposed peak cyclic load
q_{u}	ultimate capacity
$q_{\mathrm{u(dr,ref)}}$	reference ultimate drained capacity at $(v/d)_{\mathrm{ref}}$
$q_{\mathrm{u(un)}}$	ultimate undrained capacity at $V = V_{\mathrm{un}}$
$q_{\mathrm{u(un,cav)}}$	ultimate undrained capacity upon cavitation
s_{f}	shape factor
s_{u}	undrained shear strength
T	temperature
t	time
t_{a}	plate anchor thickness
t_{p}	zero crossing mean wave period
u, u_{i}	pore pressure, initial pore pressure at initial embedment depth of anchor
u_2	pore pressure at cone shoulder position
u_{cav}	cavitation pressure
u_{w}	hydrostatic pressure
V, V_{dr}, V_{un}	non-dimensional velocity, non-dimensional velocity at drained and undrained limits
V_{50}	non-dimensional velocity corresponding to 50% consolidation
v, v_{ref}	loading rate or penetration velocity, reference penetration velocity
z	penetration depth
α	anchor rotation angle (to the horizontal)
α_{cone}	unequal area ratio for cone penetrometer
α_{u}	anchor rotation angle at ultimate capacity
β	load inclination at mudline
Δz, Δz_{f}	loss in anchor embedment, loss in anchor embedment at the end of test
δ, δ_{max}	mooring line displacement, maximum mooring line displacement
δ_{u}	mooring line displacement at anchor ultimate capacity
γ, γ'	total and effective unit weight
$\dot{\gamma}$	shear rate
μ, $\mu_{20°\mathrm{C}}$	dynamic viscosity, dynamic viscosity at 20°C
ρ	density
ρ_{d}, ρ_{sat}	dry and saturated density
ρ_{min}, ρ_{max}	minimum and maximum dry density
σ'_{v}	vertical effective stress
ϕ'_{cs}	critical state friction angle

REFERENCES

Adamidis, O. & Madabhushi, G. S. P. (2015). Use of viscous pore fluids in dynamic centrifuge modelling. *Int. J. Phys. Modelling Geotech.* **15**, No. 3, 141–149.

Standards Australia (2006). AS 1289.3.5.1-06 Soil classification tests – determination of the soil particle density of a soil – Standard method. Sydney, Australia: Standards Australia.

ASTM (2006a). ASTM D4253-00: Standard test method for maximum index density and unit weight of soils using a vibratory table. American Society for Testing and Materials, West Conshohocken, PA, USA.

ASTM (2006b). ASTM D4254-00: Standard test method for minimum index density and unit weight of soils and calculation of relative density. American Society for Testing and Materials, West Conshohocken, PA, USA.

ASTM (2009). ASTM D6913-04: Standard test method for particle-size distribution (gradation) of soils using sieve analysis. American Society for Testing and Materials, West Conshohocken, PA, USA.

Been, K., Jefferies, M. G. & Hachey, J. (1991). The critical state of sands. *Géotechnique* **41**, No. 3, 365–381, https://doi.org/10.1680/geot.1991.41.3.365.

Bemben, S. M., Kalajian, E. H. & Kupferman, M. M. (1973). The vertical holding capacity of marine anchors in sand and clay subjected to static and cyclic loading. *Proceedings of the offshore technology conference*, Houston, TX, USA, paper OTC 1912.

Bhattacharya, P. & Kumar, J. (2014). Pullout capacity of inclined plate anchors embedded in sand. *Can. Geotech. J.* **51**, No. 11, 1365–1370.

Bienen, B., Klinkvort, R. T., O'Loughlin, C. D., Zhu, F. & Byrne, B. W. (2018). Suction caissons in dense sand, part I: installation, limiting capacity and drainage. *Géotechnique* **68**, No. 11, 1–47, https://doi.org/10.1680/jgeot.16.P.281.

Bolton, M. D., (1986). The strength and dilatancy of sands. *Géotechnique* **36**, No. 1, 65–78, https://doi.org/10.1680/geot.1986.36.1.65.

Bransby, M. F. & Ireland, J. (2009). Rate effects during pipeline upheaval buckling in sand. *Proc. Instn Civ. Engrs – Geotech. Engng* **162**, No. 5, 247–256.

Byrne, B. W. & Houlsby, G. T. (2002). Experimental investigations of response of suction caissons to transient vertical loading. *J. Geotech. Geoenviron. Engng* **128**, No. 11, 926–939.

Casaubieilh, P., Thiebaut, F., Bosma, B., Retzler, C., Shaw, M., Letertre, Y. & Sheng, W. (2015). Performance improvements of mooring systems for wave energy converters. In *Renewable energies offshore* (ed. C. Guedes Soares), pp. 897–904. Leiden, the Netherlands: CRC Press/Balkema.

Cassidy, M., Gaudin, C. & Randolph, M. (2012). A plasticity model to assess the keying of plate anchors. *Géotechnique* **62**, No. 9, 825–836, https://doi.org/10.1680/geot.12.OG.009.

Chow, S. H., O'Loughlin, C. D., Corti, R., Gaudin, C. & Diambra, A. (2015). Drained cyclic capacity of plate anchors in dense sand: experimental and theoretical observations. *Géotechnique Lett.* **5**, No. 2, 80–85, https://doi.org/10.1680/geolett.15.00019.

Chow, S. H., O'Loughlin, C. D., Gaudin, C., Knappett, J. A., Brown, M. J. & Lieng, J. T. (2017). An experimental study of the embedment of a dynamically installed anchor in sand. In *Proceedings of the 8th international conference of offshore site investigation and geotechnics: smarter solutions for future offshore developments (OSIG17)*, pp. 1019–1025. London, UK: Society for Underwater Technology.

Chow, S. H., O'Loughlin, C. D., Gaudin, C. & Lieng, J. T. (2018a). Drained monotonic and cyclic capacity of a dynamically installed plate anchor in sand. *Ocean Engng* **148**, 588–601.

Chow, S. H., Bienen, B. & Randolph, M. F. (2018b). Rapid penetration of piezocones in sand. In *Proceedings of the 4th international symposium on cone penetration testing (CPT'18)* (eds. M. A. Hicks, F. Pisanò and J. Peuchen), pp. 213–219. London, UK: Taylor & Francis Group.

Chow, S. H., Roy, A., Herduin, M., Heins, E., King, L. Bienen, B., O'Loughlin, C. D., Gaudin, C. & Cassidy, M. J. (2019). *Characterisation of UWA superfine silica sand. Oceans graduate school technical report*, Geo 18844. Perth, Australia: The University of Western Australia.

Chu, J., Wanatowski, D., Loke, W. L. & Leong, W. K. (2015). Pre-failure instability of sand under dilatancy rate controlled conditions. *Soils Found.* **55**, No. 2, 414–424.

Chung, S. F., Randolph, M. F. & Schneider, J. A. (2006). Effect of penetration rate on penetrometer resistance in clay. *J. Geotech. Geoenviron. Engng* **132**, No. 9, 1188–1196.

Colreavy, C., O'Loughlin, C. D. & Randolph, M. F. (2016). Experience with a dual pore pressure element piezoball. *Int. J. Phys. Modelling Geotech.* **16**, No. 3, 101–118.

Dayal, U. & Allen, J. H. (1975). The effect of penetration rate on the strength of remolded clay and sand samples. *Can. Geotech. J.* **12**, No. 3, 336–348.

Dewoolkar, M. M., Ko, H. Y., Stadler, A. T. & Astaneh, S. M. F. (1999). A substitute pore fluid for seismic centrifuge modeling. *Geotech. Test. J.* **22**, No. 3, 196–210.

Dickin, E. A. & Leung, C. F. (1983). Centrifugal model tests on vertical anchor plates. *J. Geotech. Geoenviron. Engng* **109**, No. 12, 1503–1525.

Dietz, M. S. (2000). *Developing a holistic understanding of interface friction using sand within the direct shear apparatus.* PhD thesis, University of Bristol, Bristol, UK.

Dow (Dow Chemical Company) (2002). *Methocel cellulose ethers: technical handbook*. Staines, UK: The Dow Chemical Company.

Finnie, I. M. S. & Randolph, M. F. (1994). Punch-through and liquefaction induced failure of shallow foundations on calcareous sediments. In *BOSS'94: behaviour of offshore structures* (eds. C. Chryssostomidis, M. S. Triantafyllou, A. J. Whittle and M. S. Hoo Fatt), pp. 217–230. Oxford, UK: Pergamon.

Garnier, J., Gaudin, C., Springman, S. M., Culligan, P. J., Goodings, D., Konig, D., Kutter, B., Phillips, R., Randolph, M. F. & Thorel, L. (2007). Catalogue of scaling laws and similitude questions in geotechnical centrifuge modelling. *Int. J. Phys. Modelling Geotech.* **7**, No. 3, 1–23.

Gaudin, C., Tham, K. H. & Ouahsine, S. (2009). Keying of plate anchors in NC clay under inclined loading. *Int. J. Offshore Polar Engng* **19**, No. 2, 135–142.

Heurlin, K., Rességuier, S., Melin, D. & Nilsen, K. (2015). Comparison between FEM analyses and full-scale tests of fluke anchor behavior in silty sand. In *Frontiers in offshore geotechnics III* (ed. V. Meyer), pp. 875–880. Leiden, the Netherlands: CRC Press/Balkema.

Hölscher, P., van Tol, A. F. & Huy, N. Q. (2012). Rapid pile load tests in the geotechnical centrifuge. *Soils Found.* **52**, No. 6, 1102–1117.

McManus, K. J. & Davis, R. O. (1997). Dilation-induced pore fluid cavitation in sands. *Géotechnique* **47**, No. 1, 173–177, https://doi.org/10.1680/geot.1997.47.1.173.

Merifield, R. & Sloan, S. (2006). The ultimate pullout capacity of anchors in frictional soils. *Can. Geotech. J.* **43**, No. 8, 852–868.

Merifield, R., Lyamin, A. V. & Sloan, S. (2005). Stability of inclined strip anchors in purely cohesive soil. *J. Geotech. Geoenviron. Engng* **313**, No. 6, 792–799.

Muir Wood, D. W. (1990). *Soil behaviour and critical state soil mechanics.* Cambridge, UK: Cambridge University Press.

Murray, E. F. & Geddes, J. D. (1989). Resistance of passive inclined anchors in cohensionless medium. *Géotechnique* **39**, No. 3, 417–431.

O'Loughlin, C. D. & Barron, B. (2012). Capacity and keying response of plate anchors in sand. In *Proceedings of the 7th international conference on offshore site investigation & geotechnics*, pp. 649–655. London, UK: Society for Underwater Technology.

Ovesen, N. K. & Stromann, H. (1972). Design method for vertical anchor slabs in sand. In *Proceedings of the speciality conference on performance of earth and earth-supported structures*, vol. 1, part 2, pp. 1481–1500. New York, NY, USA: American Society of Civil Engineers.

Palmer, A. C. (1999). Speed effects in cutting and ploughing. *Géotechnique* **49**, No. 3, 285–294, https://doi.org/10.1680/geot.1999.49.3.285.

Pan, K., Yang, Z. X. & Xu, T. T. (2018). Impact of static preshearing on undrained anisotropy and shear characteristics of sand. *Int. J. Geomech.* **18**, No. 12, 04018162.

Randolph, M. F. (2016). New tools and directions in offshore site investigation. *Aust. Geomech. J.* **51**, No. 4, 81–92.

Robinson, S., Brown, M. J., Matsui, H., Brennan, A., Augarde, C. E., Coombs, W. & Cortis, M. (2019). Centrifuge testing to verify scaling of offshore pipeline ploughs. *Int. J. Phys. Modelling Geotech.* **19**, No. 6, 305–317.

Song, Z. & Hu, Y. (2009). Plate anchor keying under inclined pullout in clay: observation and estimation. In *Proceedings of the 17th international conference on soil mechanics and geotechnical engineering* (eds M. Hamza, M. Shahien and Y. El-Mossallamy), vol. 1, pp. 708–711. Amsterdam, the Netherlands: IOS Press.

Stewart, D. P., Chen, Y. R. & Kutter, B. L. (1998). Experience with the use of methylcellulose as a viscous pore fluid in centrifuge. *ASTM Geotech. Test. J.* **21**, No. 4, 365–369.

Suzuki, Y. & Lehane, B. M. (2014). Rate dependence of q_c in two clayey sands. *Proceedings of the 3rd international symposium on cone penetration testing (CPT14)*, Las Vegas, NV, USA, pp. 411–418.

Verdugo, R. & Ishihara, K. (1996). The steady state of sandy soils. *Soils Found.* **36**, No. 2, 81–91.

Wang, D., Hu, Y. & Randolph, M. (2011). Keying of rectangular plate anchors in normally consolidated clays. *J. Geotech. Geoenviron. Engng* **137**, No. 12, 1244–1253.

Watanabe, K. & Kusakabe, O. (2013). Reappraisal of loading rate effects on sand behavior in view of seismic design for pile foundation. *Soils Found.* **53**, No. 2, 215–231.

White, D. J., Cheuk, C. Y. & Bolton, M. D. (2008). The uplift resistance of pipes and plate anchors buried in sand. *Géotechnique* **58**, No. 10, 771–779, https://doi.org/10.1680/geot.2008.3692.

Zhu, H. & Randolph, M. F. (2011). Numerical analysis of a cylinder moving through rate-dependent undrained soil. *Ocean Engng* **38**, No. 7, 943–953.

Zhu, F., Bienen, B., O'Loughlin, C., Cassidy, M. J. & Morgan, N. (2019). Suction caisson foundations for offshore wind energy: cyclic response in sand and sand over clay. *Géotechnique* **69**, No. 10, 924–931, https://doi.org/10.1680/jgeot.17.P.273.